International Journal for Housing Science and Its Applications
Publish August 6, 2025. Volume 46, Issue 3 Pages 5940-5952

https://doi.org/10.70517/ijhsa463511

Correlation between lightning activity and topographic features in Inner Mongolia: a study based on geographic information system and spatial interpolation

Shi Jin[1], Amuersana[1,*], Nanjisangmo[2], Lu Chao[1], Danping Wang[1] and Xuan Li[1]
[1] Meteorological Disaster Prevention Center, Hohhot Meteorological Bureau, Hohhot, Inner Mongolia, 010020, China
[2] Research Department, Inner Mongolia People's Hospital, Hohhot, Inner Mongolia, 010010, China
Corresponding authors: (e-mail: amuersana@outlook.com).

Abstract Complex and diverse topography and frequent lightning activities in Inner Mongolia pose a serious threat to agricultural production and infrastructure safety. Based on geographic information system and spatial interpolation techniques, this study explores the correlation between lightning activity and terrain features in Inner Mongolia and establishes an accurate prediction model. The study adopts the improved DBSCAN algorithm to cluster lightning activities, combines the kernel density estimation to adaptively determine the clustering parameters, utilizes kriging interpolation to determine the lightning fall area, and fits the thunderstorm movement trajectory through the least squares method. The experimental results show that the improved DBSCAN algorithm has an average offset error of 1.16 km on thundercloud center of mass prediction, which is significantly better than the linear extrapolation method (1.92 km) and the least squares method (3.09 km). The prediction accuracy is more than 80% and the false alarm rate is controlled below 40%. The topographic analysis found that the frequency of intensity lightning is highest on the northeast slope; the influence of slope on lightning density decreases gradually with the increase of lightning intensity, and Class I to III lightning is prone to occur on steep slopes. The study can provide scientific basis for the layout of lightning protection facilities, lightning disaster risk assessment and early warning in Inner Mongolia, and has practical application value for enhancing regional disaster prevention and mitigation capability.

Index Terms lightning activity, topographic features, DBSCAN clustering algorithm, spatial interpolation, geographic information system, lightning prediction

I. Introduction

Lightning is a common natural phenomenon, which occurs frequently and is very harmful. Lightning disaster is listed by the United Nations as “one of the ten most serious natural disasters”, and also identified by the International Electrotechnical Commission (IEC) as “a major public hazard in the era of electronic” [1]. The powerful destructive nature of lightning originates from the strong physical effects such as current, high temperature, electromagnetic radiation and shock wave, etc., which can directly or indirectly cause casualties, and cause serious damage to buildings, distribution systems and communication equipment, and also cause forest and grassland fires and other disasters, which are very harmful to people's lives and properties [2]-[5].

Inner Mongolia Autonomous Region is a vast area, belonging to one of the provinces where thunderstorm activities and lightning disasters occur more frequently, characterized by high frequency and wide distribution. Lightning disasters have become the third major meteorological disaster after heavy rainfall and flooding, wind and hail. In the past 15 years, about 653 lightning accidents occurred in the region, with an average of 43.5 accidents per year, and the direct economic losses caused by lightning strikes were about 175.16 million yuan, with an average of about 11.678 million yuan per year, and lightning strikes caused about 15 casualties per year [6]-[8]. Carrying out relevant research on the characterization of lightning activity and lightning disaster can provide an objective scientific basis for strengthening the risk management of lightning disaster and improving the level of lightning disaster prevention and mitigation. A number of studies have shown that terrain is a factor that has a large impact on lightning activity, mountains, forests and buildings may affect the distribution of lightning, lightning generally occurs in the terrain open areas, it is smaller but more frequent, and different topographic features have different impacts on terrain [9]-[12]. Research on the correlation law of lightning activity and topography is very important for the development of lightning protection work in the power system, which can provide a scientific basis for the relevant

departments to strengthen the management of lightning protection and disaster reduction, and improve the ability of lightning protection and disaster reduction.

Geographic information system (GIS) is the use of computer storage, processing of geographic information, a technology and tools. It is supported by computer software and hardware, various resource information and environmental parameters according to spatial distribution or geographical coordinates, in a certain format and classification code input, processing, storage, output, to meet the application needs of human-computer interactive information system, in terrain analysis, environmental protection, ecological monitoring, urban management, disaster prediction, emergency response and other aspects of the role played a positive role [13]-[17]. With the rapid development of GIS technology, spatial interpolation method as an important tool in GIS. As the spatial interpolation method is to predict and project the data values of the unknown region through the known spatial data points, thus revealing the spatial distribution characteristics and change rules, it has been widely used in many fields such as geology, agriculture, meteorology, environmental monitoring and so on [18]-[21]. The two provide a basis for exploring the connection between lightning activity and topographic features.

Lightning activity is a common strong convective weather phenomenon in nature, which has a significant impact on human production and life and socio-economic development. Due to its unique geographic location and diverse topographic features, lightning activity in Inner Mongolia shows obvious spatial and temporal distribution characteristics, and agricultural losses, damage to power facilities and casualties caused by lightning occur frequently every year. Understanding the correlation between lightning activity and topographic features and establishing accurate lightning prediction models are of great significance to improve lightning disaster defense capability and reduce disaster losses. Traditional lightning prediction methods mainly rely on meteorological observation data and empirical models, with limited accuracy and poor timeliness. With the development of geographic information system (GIS) technology and spatial analysis methods, it has become possible to predict lightning activity by combining topographic factors. In this study, based on the lightning location data, thunderstorm day data, precipitation data, and severe convective weather hazard data for 2019-2022 in Inner Mongolia, the correlation between lightning activity and topographic features such as elevation, slope direction, and slope gradient is systematically analyzed by using geographic information system (GIS) and spatial interpolation techniques, and a prediction model for lightning activity based on the improved DBSCAN algorithm is constructed. The DBSCAN algorithm, as a density-based clustering method, does not need to specify the number of classes in advance, and is able to effectively identify clusters of arbitrary shapes, which is suitable for the identification and analysis of thunderstorm clouds. In this study, the parameters of the DBSCAN algorithm are optimized by kernel density estimation, which improves the adaptivity and accuracy of the algorithm. In terms of prediction, the study combines the Kriging interpolation and the least squares method to realize the accurate prediction of the moving trajectory of thunderstorm clouds and the area of mine fall. In terms of terrain correlation analysis, the study divides Inner Mongolia into plains, hills, basins and mountains according to elevation, nine categories according to slope direction, and seven levels according to slope gradient, and systematically examines the distribution patterns of lightning activities of different intensities under various terrain conditions. It is found that there is an obvious correlation between lightning activity and terrain characteristics, and lightning of different intensities show different distribution characteristics under different terrain conditions. Based on the results of the study, this paper puts forward suggestions for the location of flammable and explosive places, the setting of lightning protection level, the lightning safety inspection cycle, and the setting of lightning shelters, which provides a scientific basis for the lightning disaster defense work in Inner Mongolia. This study not only enriches the theoretical study of the relationship between lightning activity and topography, but also provides technical support for lightning disaster risk assessment, early warning and defense in Inner Mongolia, and has important practical application value for enhancing the regional disaster prevention and mitigation capabilities.

II. Algorithm and process for predicting lightning activity in Inner Mongolia

II. A. Clustering Algorithm Flow

II. A. 1) DBSCAN algorithm

In this paper, the DBSCAN algorithm [22] is selected to cluster and sort the lightning activities in Inner Mongolia without specifying the number of classes of the battery in advance:

1) Input battery feature vector $D=\{x_1,\cdots,x_4\}$ with parameters Eps, $MinPts$.

2) Find the Eps neighborhood subsample set of all lightning activity samples x_i by means of the distance metric, and if the number of samples in the subsample set satisfies $N_{Eps}(x_i)\geq MinPts$, the lightning activity x_i is added to the core object sample set Ω. If it is not satisfied, mark the cell x_i as a boundary point or noise point.

3) In the core object collection Ω, randomly select a lightning activity core object o, establish a new cluster sample collection C_1, and add all lightning activities in its Eps neighborhood to the cluster C_1; check all lightning

activities in the cluster C_1 in its Eps neighborhood to be added to C_1; repeat the check until no new lightning activity can be added. Update the core object set $\Omega = Q - C_1$.

4) Randomly select a lightning activity core object o in the updated core object set Ω, repeat step 3) until the core object set Ω is empty, and output the cluster division result $\{C_1, C_2, \cdots, C_n\}$.

II. A. 2) Kernel density estimation

The accuracy of the DBSCAN clustering algorithm is closely related to the settings of the parameters Eps and $MinPts$. A very small setting of Eps or a very large setting of $MinPts$ may result in too many or even all points being labeled as noise; when Eps is set very large or $MinPts$ is set very small, it may result in a single cluster of all sample points.

For the cells to be clustered, the clustering results are made more accurate by setting the appropriate DBSCAN algorithm parameters based on the sample densities according to the kernel density estimation of the distribution density function solved for a given set of characteristic sample points. The effect of the size of the kernel density estimation window width h on the kernel density estimation is consistent with the performance of Eps in the clustering process. Therefore, in this paper, the DBSCAN algorithm parameter Eps is converted to the optimization of the window width value h in kernel density estimation. By determining the size of the window width value h, the appropriate value of the parameter Eps can be determined.

The mean square error method is commonly used in kernel density estimation to study the choice of window width, using the mean square error function MISE(h) to reflect the goodness of the kernel density estimation.

$$MISE(h) = \frac{\int K^2(x)dx}{nh} + \frac{h^4\sigma^4\int\left[f^n(x)\right]^2dx}{4} + o\left(\frac{1}{nh} + h^4\right) \tag{1}$$

Approximation:

$$MISE(h) = \frac{\int K^2(x)dx}{nh} + \frac{h^4\sigma^4\int\left[f^n(x)\right]^2dx}{4} \tag{2}$$

where $K(x)$ is the kernel density function; h is the window width value; and σ is the sample variance.

From Eq. (2), it can be seen that the kernel density estimation MISE(h) is required to be optimized, i.e., to solve for the minimum value of MISE(h). The optimal window width h is obtained by deriving Eq. (2) and making the first order inverse equal to zero, i.e.:

$$h = \left[\frac{\int K^2(x)dx}{n\sigma^4\int(f^n(x))^2dx}\right]^{1/5} \tag{3}$$

Defined for ease of calculation:

$$R[f(x)] = \int f(x)dx \tag{4}$$

For the unknown quantity $R[f(x)]$, B.W. Sliverman proposed the thumb rule, which is obtained by replacing $f(x)$ with a normal density whose variance matches the estimated variance:

$$Eps = h \approx [4/(3n)]^{1/5}\hat{\sigma} \tag{5}$$

After determining the appropriate Eps, equation (6) is used to determine the appropriate $MinPts$.

$$\min Pts = \sum_{i=1}^{n} K\left(\frac{x - x_i}{Eps}\right) \tag{6}$$

II. B.Lightning activity prediction algorithm and process

II. B. 1) Spatial interpolation

Following the principle of Kriging interpolation [23], the general formula is as follows:

$$Z(x_0) = \sum_{i=1}^{n}\lambda_i Z(x_i) \quad (i = 1, 2, \cdots, n) \tag{7}$$

where, $Z(x_0)$ is the predicted value at x_0, $Z(x_i)$ is the true value at x_i, and λ_i is the weight coefficients to be sought.

Assuming that $Z(x)$ satisfies the second-order smoothness condition throughout the sample space, based on the unbiasedness requirement: $E[Z^*(x_0)] = E[Z(x_0)]$, which can be deduced from Eq. (8):

$$\sum_{i=1}^{n} \lambda_i = 1 \tag{8}$$

Minimize the estimation variance under unbiased conditions, i.e:

$$Min\left\{Var\left[Z^*(x_0) - Z(x_0)\right] - 2\mu\sum_{i=1}^{n}(\lambda_i - 1)\right\} \tag{9}$$

where μ is the Lagrange multiplier.

It can be obtained that the matrix form when solving for the weight coefficients λ_i expressed in terms of the variational function $\gamma(x_i, x_j)$ is:

$$\begin{bmatrix} \gamma_{11} & \gamma_{12} & \cdots & \gamma_{1n} & 1 \\ \gamma_{21} & \gamma_{22} & \cdots & \gamma_{2n} & 1 \\ \vdots & \vdots & \ddots & \vdots & \vdots \\ \gamma_{n1} & \gamma_{n2} & \cdots & \gamma_{nn} & 1 \\ 1 & 1 & \cdots & 1 & 0 \end{bmatrix} \begin{bmatrix} \lambda_1 \\ \lambda_2 \\ \vdots \\ \lambda_n \\ 0 \end{bmatrix} + \begin{bmatrix} \mu \\ \mu \\ \vdots \\ \mu \\ 0 \end{bmatrix} = \begin{bmatrix} \gamma_{01} \\ \gamma_{02} \\ \vdots \\ \gamma_{0n} \\ 1 \end{bmatrix} \tag{10}$$

The inverse of the matrix yields the weighting coefficients $\lambda_i (i = 1, 2, ..., n)$, from which the estimate at sampling point x_0 can be obtained $Z^*(x_0)$. Where the variational function is:

$$\gamma(x_i, x_j) = \gamma(x_i - x_j) = E[Z(x_i) - Z(x_j)]^2 / 2 \tag{11}$$

II. B. 2) Least Squares

Usually, when we study the interrelationships between variables (x, y), we will start from a series of data $(x_i, y_i)(i = 1, 2, \cdots, m)$ in groups, plot these points in an $x - y$ coordinate system, and then use a curve to represent the relationship between these variables, which is the curve fitting problem. The least squares method [24] (also known as the least square method) is one of the more common curve fitting methods, which applies the principle of squaring and minimizing the sum of errors in the fitting process to match the best function of the data.

Assuming the data is $(x_i, y_i)(I = 1, 2, \cdots, m)$ and the expression is $y = f(x, a_0, \cdots, a_n)$, the sum of squares of error expression is:

$$F(a_0, \cdots, a_n) = \sum_{i=1}^{m}\left[f(x_i, a_0, \cdots, a_n) - y_i\right]^2 \tag{12}$$

where, $a_0, \cdots, a_n$ is the pending parameter of the curve and m is the given number of points. The pending parameters can be obtained by solving the system of derivative equations, which is necessary to obtain the extreme values:

$$\frac{\partial F}{\partial a_k} = 0, (k = 0, 1, \cdots, n) \tag{13}$$

Based on equation (13), $n+1$ equations can be obtained, and the pending parameters of the curve $y = f(x, a_0, \cdots, a_n)$ can be found out immediately. In this paper, the variable (x, y) is the latitude and longitude of the thunderstorm cloud center, and the curve obtained is the thunderstorm cloud motion track.

II. B. 3) Prediction Algorithm Flow

The improved DBSCAN clustering algorithm, which can adaptively determine the clustering parameters, and the weighted Euclidean distance is conducive to the elimination of noise points and the retention of core points, is more suitable for the identification and clustering of thunderstorm clouds, and lays a good foundation for further thunderstorm prediction. The flowchart of thunderstorm cloud identification is shown in Fig. 1.

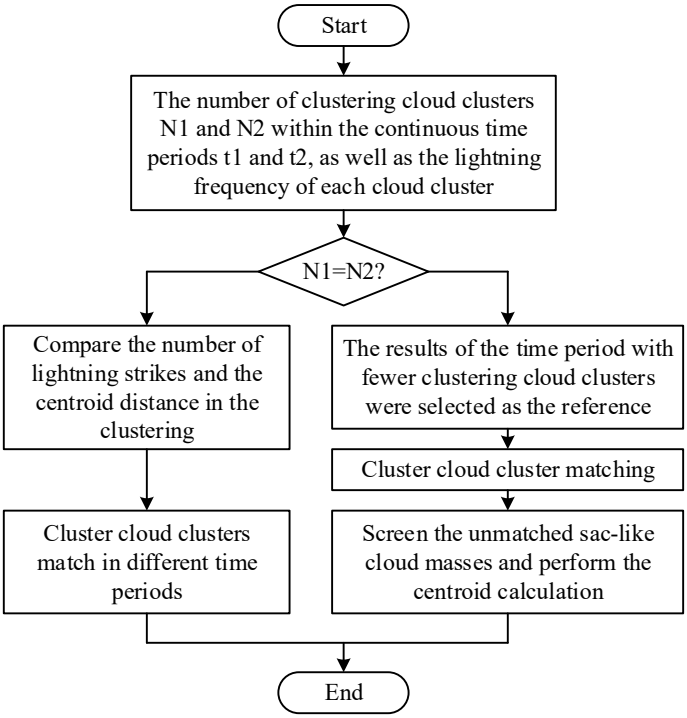

Figure 1: Thundercloud mass recognition flow chart

The specific steps for thunderstorm warning are as follows:

(1) Apply the trans-Gaussian kernel density estimation to determine the parameters ε and MinPts, and select the ground flash data set D.

(2) Select a point as the starting point, mark p, and further search the $\varepsilon-$ neighborhood of the point via the weighted Euclidean distance formula to determine whether it is a core point.

(3) If the point is a core point, create a new clustering cluster C, and find out all the points in the neighborhood with direct density reachable to join the candidate set N.

(4) Determine whether all points in the dataset N are traversed or not, if not, repeat steps (2)-(4).

(5) Merge all points with reachable density and extend cluster C.

(6) Output the set of target clusters to generate thunderstorm clouds.

(7) Find the center of each cluster and apply kriging interpolation to determine the thunderstorm region.

(8) Apply least squares fitting to the center of thunderstorms for multiple time periods to generate the location of the thunderstorm motion track.

(9) Calculate the direction and speed of thunderstorm movement, and predict the location of thunderstorms and the area of falling mines for the next time period.

II. C. Sources of information

II. C. 1) Flash localization data

Graphic display client is a combination of geographic information systems (GIS) using high-tech web communication functions, digital analysis of data into a graphical way, timely calculation of cloud-to-ground flash occurrence time, geographic location, lightning parameters. Receive lightning data in real time, realize the query and statistical function of the data. Through the lightning monitoring system is very good to monitor the lightning data into colorful graphics presented at a glance, so that people can analyze the data in a timely manner is conducive to the timely application of lightning information.

II. C. 2) Information on thunderstorm days

A thunderstorm day is defined as a day in which thunder is heard (once or more than once), regardless of its duration, and is counted as a thunderstorm day in days. In this paper, the data of thunderstorm days observed manually by six basic meteorological stations (Hohhot suburb, Wuchuan, Helinger, Tumet Left Banner, Qingshuihe, and Toketo County) for surface meteorological operations from 1983 to 2022 are utilized for the study.

II. C. 3) Regional precipitation data

This paper utilizes the 24h corresponding precipitation data from 1983 to 2022 at six meteorological observation stations, the precipitation is measured by the tipping bucket rain sensor, currently used in Inner Mongolia is the SL3-1 type double tipping bucket rain sensor, the tipping bucket rain sensor is a common instrument for measuring rainfall, at the same time, it can be converted into the rainfall expressed in the form of switches to the output of digitized information to meet the information transmission, processing, recording and display needs.

II. C. 4) Data on severe convective weather hazards

Data on agricultural disasters caused by strong convective weather in the Hohhot area from 2011 to 2022 provided by the Hohhot Meteorological Bureau, specifically including the types of strong convective disasters, affected crops, damaged areas, economic losses and other information.

II. C. 5) Lightning hazard data

Data on agricultural disasters caused by strong convective weather in the Hohhot area from 2011 to 2022 provided by the Hohhot Meteorological Bureau, specifically including the types of strong convective disasters, affected crops, damaged areas, economic losses and other information.

III. Correlation analysis between predicted lightning activity and topographic features in Inner Mongolia

III. A. Forecast of lightning activity in Inner Mongolia

Python3.10 was used as the platform for program simulation, and ArGIS10.2 was used as the development tool. The original data were obtained from the thunderstorm data in the Inner Mongolia grassland region monitored by the lightning detection and positioning system. Due to the large amount of data, the thundercloud center-of-mass movement data in 2021-2022 were intercepted as the historical data to train the improved DBSCAN algorithm to verify the effectiveness of the prediction with the strong thunderstorm data occurring on August 5, 2021, from 8:05-8:35 located in the range of E125.0°-E127.5°, N23.2°-N27.3°. N27.3° range of strong thunderstorm data occurring in the range of N27.3° to verify the effectiveness of the prediction. The trained and improved DBSCAN algorithm is then used to predict the thundercloud center-of-mass moving trajectories in the next 17 min. The past thundercloud centers-of-mass for three consecutive time periods are used as input values, and the output values are the predicted centers-of-mass of thunderclouds for three consecutive time periods in the next 17 min.

After clustering the separate noise points are eliminated, and the remaining falling thunder points are compact, after clustering the separate noise points are eliminated, and the remaining falling thunder points are compact and dense, it can be clearly seen that three thunderstorm cloud clusters, C1, C2, and C3, are formed, and all three clusters have a tendency to move toward the southeast. The centers of mass of clouds C1, C2, and C3 in the three time periods are calculated, and the centers of mass of the clustered clouds in each time period are obtained as shown in Table 1.

Table 1: The results of the cluster of the cluster

Time	Cluster cloud	Center of mass coordinates	
		Longitude/°	Latitude/°
8:05-8:10	C1	128.721	27.348
	C2	128.097	25.815
	C3	128.184	24.956
8:10-8:15	C1	128.822	27.214
	C2	128.194	25.722
	C3	128.415	24.982
8:15-8:20	C1	128.933	27.847
	C2	128.297	25.673
	C3	128.428	24.857

Calculating the actual offset distance of each prediction method is shown in Table 2, the improved DBSCAN algorithm has the smallest average offset error on the prediction of thundercloud center of mass, with the average offset error within 2km, which is better than the other two algorithms.

Table 2: The parties act to predict the offset error

Thunder number	Forecast time	Deviation error /km		
		Linear extrapolation	Least squares	Improved DBSCAN
C1	8:20-8:25	1.84	2.22	0.86
	8:25-8:30	3.62	5.08	1.14
	8:30-8:35	2.29	5.29	1.79
C2	8:20-8:25	0.64	1.18	0.51
	8:25-8:30	1.49	2.91	0.92
	8:30-8:35	1.67	3.79	1.51
C3	8:20-8:25	2.85	2.37	0.96
	8:25-8:30	0.81	2.24	1.14
	8:30-8:35	2.09	2.75	1.57
Mean value		1.92	3.09	1.16

Based on the reference range of the thundercloud obtained by IDW interpolation and the center of mass of the thundercloud predicted by the improved DBSCAN algorithm, we can dynamically predict the moving trajectory of the thundercloud in the next 17 min as shown in Fig. 2. After predicting the center of mass of the thundercloud, the size and shape of the thundercloud need to be reproduced, and the thundercloud is basically stable and no longer continues to expand its lightning strike range after the thundercloud continues to fall for 5 min. The inverse distance-weighted interpolation is performed with the time period of 8:15-8:20 to obtain the contour and range of the thundercloud.

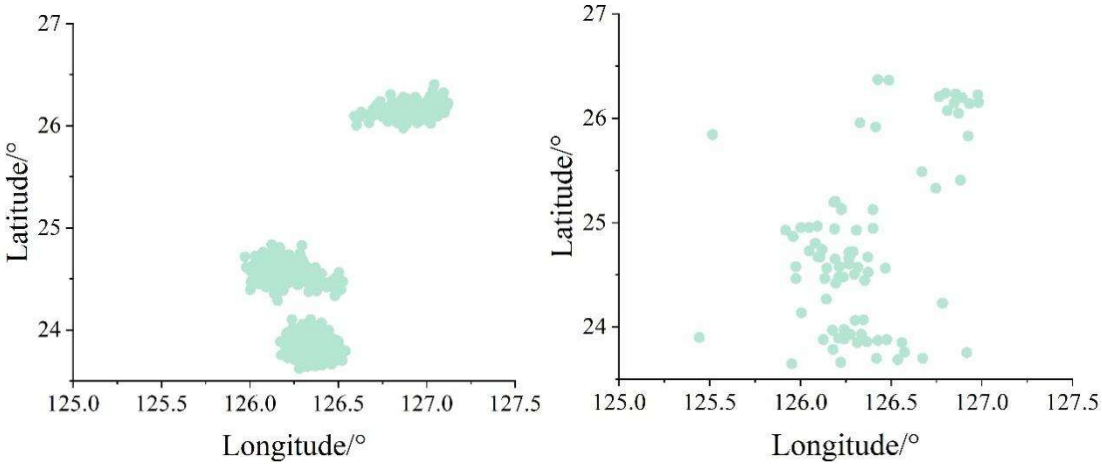

(a) 8:20-8:25 Predict the lightning strike area (b) 8:20-8:25 Actual lightning strike area

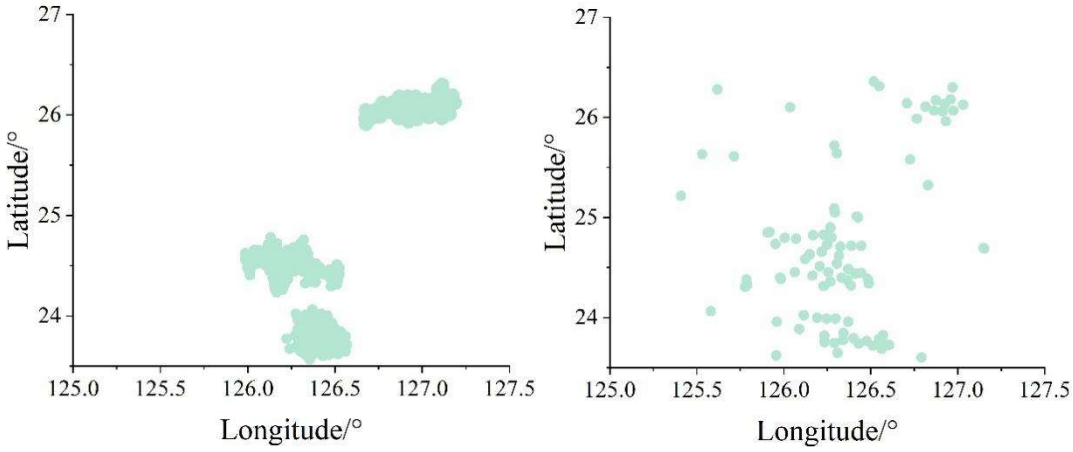

(c) 8:25-8:30 Predict the lightning strike area (d) 8:25-8:30 Actual lightning strike area

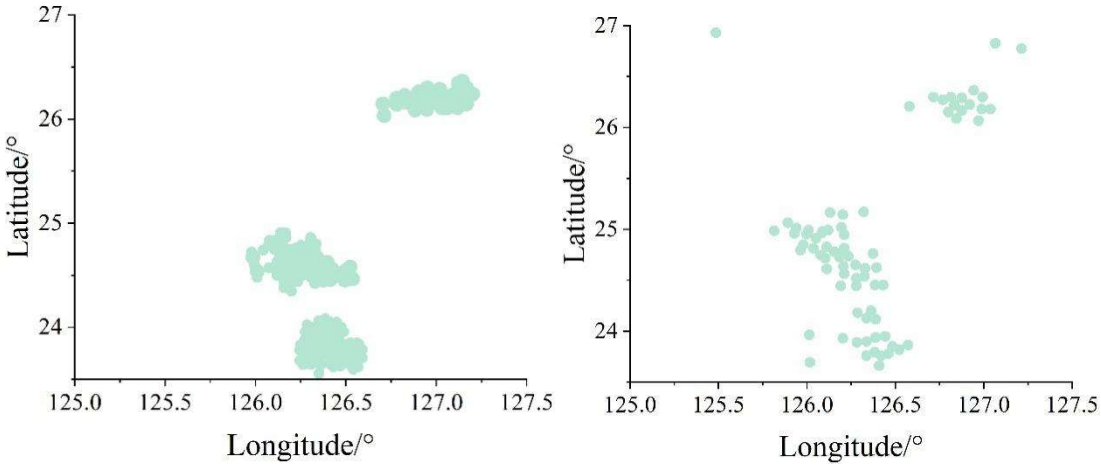

(e) 8:25-8:30 Predict the lightning strike area (f) 8:25-8:30 Actual lightning strike area

Figure 2: Ray cloud's prediction range is compared to the actual fall

The results of calculating the prediction accuracy in each time period are shown in Table 3, where the number of predicted lightning falls is the number of lightning that falls within the prediction range, and the total number of lightning falls for this time period is the total number of lightning falls. The accuracy is the ratio of the number of lightning falling into the predicted range to the total number of lightning.

Due to the relative expansion of the thundercloud range after the interpolation of the inverse distance weights, the false alarm rate becomes an important indicator to assess whether the predicted lightning fallout area can truly and reasonably reflect the thundercloud mass, and the false alarm rate of the lightning prediction for each time period is shown in Table 4. The false alarm rate is the ratio of the number of false alarm grids to the total number of predicted lightning grids, and the number of false alarm grids is the number of grids that fail to correctly predict lightning. Due to the large prediction range, the grid division spacing is chosen to be 0.05°. From Table 3 and Table 4, it can be seen that the prediction accuracy of this prediction method is more than 80%, and the false alarm rate is below 40%.

Table 3: lightning prediction accuracy

Forecast time	Forecast drop number	Thunderbolt	Accuracy rate /%
8:20-8:25	182	204	89.22%
8:25-8:30	193	231	83.55%
8:30-8:35	211	252	83.73%

Table 4: lightning prediction accuracy

Forecast time	Virtual police grid number	Grid total	Alarm rate /%
8:20-8:25	67	221	30.32%
8:25-8:30	83	221	37.56%
8:30-8:35	91	221	41.18%

III. B. Correlation analysis between lightning activity and terrain features

III. B. 1) Effect of altitude on lightning activity at different intensity levels

Based on the terrain classification convention will be plains (h<200m), hills (200m $\leqslant$ h<500m), basins (500m $\leqslant$ h<1000m), and mountains (h$\geqslant$1000m) in the study area, with plains, hills, basins, and mountains accounting for 26.71%, 42.92%, 24.83%, and 5.54% of the area, respectively. Inner Mongolia is dominated by hills, and the area of high mountains accounts for the least.

The average annual frequency and density of lightning of each intensity in the study area from 2019 to 2022 are shown in Figure 3. As can be seen from Figure 3, the frequency and interval area share of each intensity of lightning are basically consistent with respect to the change in elevation, indicating that the larger the interval area share, the more lightning occurs within the region.

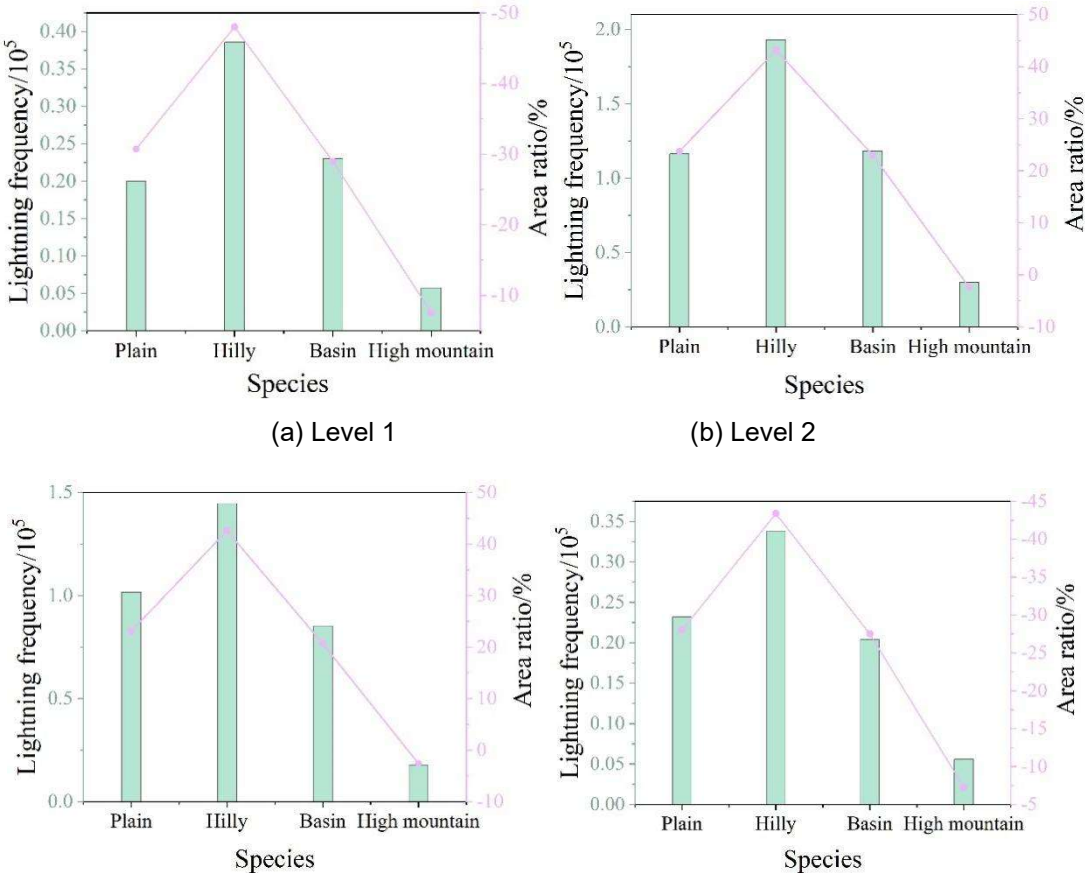

Figure 3: Different intensity thunderstorms vary with altitude

III. B. 2) Influence of slope orientation on lightning activity at different intensity levels

The slope direction is divided into 9 categories, and the statistical results of each slope direction interval and the area share of the interval where it is located are shown in Table 5, and the distribution area of each slope direction in Inner Mongolia does not differ much.

Table 5: The classification and area ratio of the slope of the sea level

Slope classification	Elevation interval /(°)	Area ratio /%
Flatness	0	0.37
Northern Slope	(0,23.4], (341.2,360]	12.54
Northeast slope	(23.4,68.2]	11.88
East slope	(68.2,114.7]	12.67
Southeast slope	(114.7,159.1]	13.74
South slope	(159.1,211.6]	12.94
Southwest slope	(216.6,255.3]	11.97
Western slope	(255.3,295.7]	12.26
Northwest slope	(295.7,344.2]	13.27

Statistics on the frequency and density of lightning of each intensity in Inner Mongolia with the change characteristics of slope direction in 2019-2022 are shown in Figure 4. As can be seen from Figure 4, there are differences in the density distribution of each intensity of lightning in each slope direction, and this paper defines the slope direction with the highest and second highest density values of each intensity of lightning as the prone area, and the Class I (weak) lightning prone area is the northeast slope and southwest slope; the Class II (moderate) lightning prone area is the northeast slope and southwest slope; the Class III (strong) lightning prone area is the northeast slope and northwest slope; and the Class IV (very strong) lightning prone area is the northeastern slope,

south slope. In general, the lightning prone areas in Inner Mongolia are the northeast slope, south slope, southwest slope and northwest slope. The reason for the above phenomenon may be that Inner Mongolia is affected by the subtropical monsoon climate, and the prevailing southwestern monsoon is easily triggered by the convection on the windward side due to the uplift of the terrain.

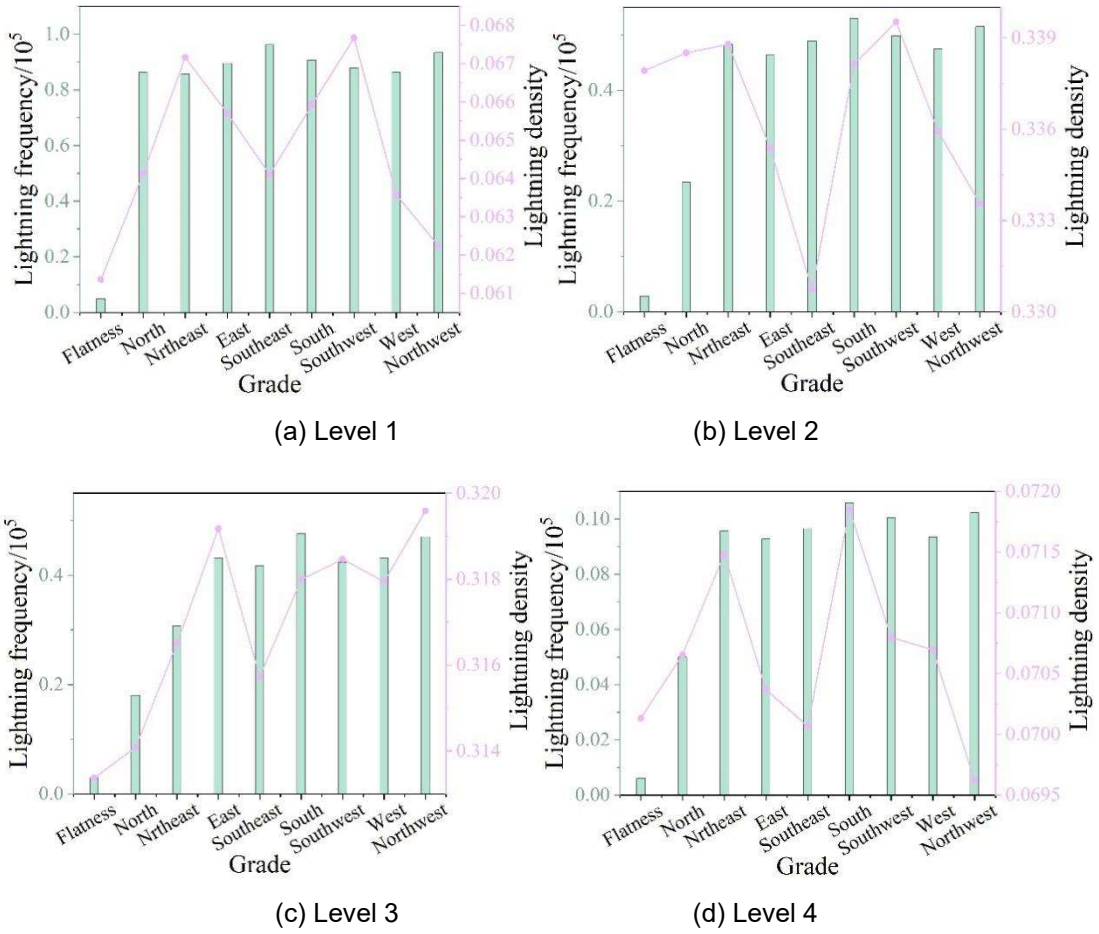

(a) Level 1 (b) Level 2

(c) Level 3 (d) Level 4

Figure 4: Different intensity lightning frequency, density varies with slope

III. B. 3) Effect of slope on lightning activity at different intensity levels

Slope classes were classified according to the slope classification method applied by the International Geographical Union Commission on Geomorphological Surveys and Geomorphological Cartography on detailed geomorphological mapping, and the statistics of each slope classification and area share are shown in Table 6.

Table 6: The classification of each slope and the product ratio

Type	Slope interval /°	Area ratio /%
Plain	[0,0.5)	1.23
Micro slope	[0.5,3)	9.63
Slow slope	[3,6)	16.37
Slope	[6,17)	39.23
Steep slope	[17,37)	36.09
Steep slope	[37,58)	0.95
Vertical wall	[58,93]	0.01

Statistics on the frequency and density of lightning of each intensity in Inner Mongolia from 2019-2022 are characterized with slope as shown in Fig. 5. Considering that the three slope intervals of plains, craggy slopes, and vertical walls may be more contingent and prone to discrepancies with the overall pattern due to the low frequency of recorded lightning and small area share, these three slopes are not included in the analysis of this study.

It can be seen that the density of Class IV (very strong) lightning does not change with slope, while the density of the other three intensities changes more significantly with slope: the density of Class I (weak) lightning increases almost linearly with slope; The density of Class II (moderate) lightning varies with slope in a V-shape; the density of Class III (strong) lightning varies with slope in a trough shape; The density of Class IV (very strong) lightning, on the other hand, basically does not vary with slope. Therefore, it can be seen that the influence of slope on the density of lightning is less and less obvious with the increase of lightning intensity. Statistics on the susceptibility of each intensity of lightning to occur on slopes show that Class I (weak), Class II (moderate), and Class III (strong) lightning are susceptible to occur on steep slopes, and Class IV (very strong) lightning has the same probability of occurring on all slopes.

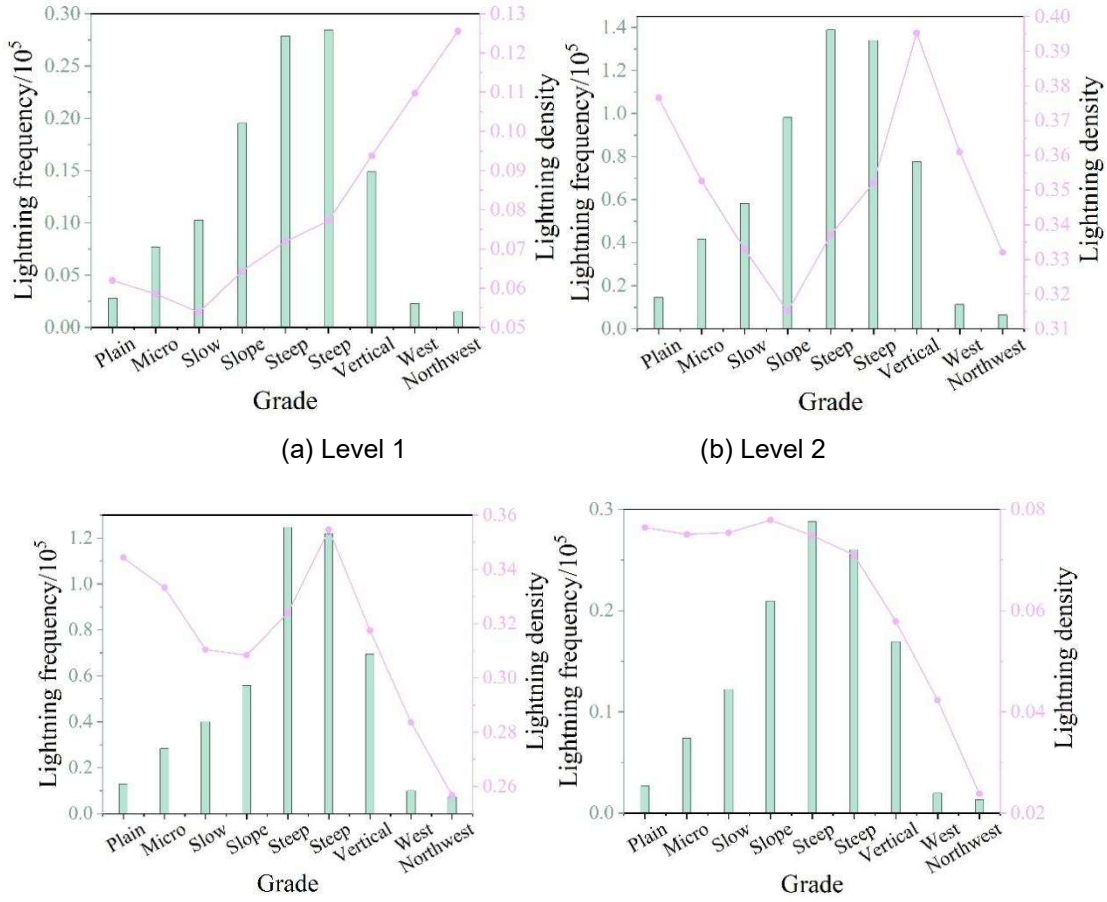

(a) Level 1 (b) Level 2

(c) Level 3 (d) Level 4

Figure 5: Different intensity lightning frequency, density varies with slope

Combining the results of the study and in connection with the actual environment, the following suggestions are made in four aspects: (1) the sites of flammable and explosive places, large-scale farms, and warehouses of hazardous chemicals should avoid the terrains prone to strong lightning and extremely strong lightning; (2) when the sites cannot avoid the terrains prone to strong lightning and extremely strong lightning, the lightning protection level of buildings and structures should be increased, and the lightning disaster risk assessment should be carried out in the pre-design stage; (3) the lightning protection facilities (catching facilities) of buildings and structures constructed in the areas prone to strong lightning and extremely strong lightning should be improved. structures of lightning protection level, and in the pre-design of lightning disaster risk assessment; (3) construction in the strong lightning, very strong lightning prone terrain area of the buildings and structures of lightning protection facilities (flashover, surge protector, etc.) are more prone to aging, attenuation, and therefore the need to strengthen the inspection patrol, it is recommended to carry out half a year of lightning safety inspection (4) construction in the strong lightning, very strong lightning prone terrain areas of the Tourist attractions, large-scale activities, such as squares, should be set up to prevent lightning shelter for the masses in a timely and effective hedge.

IV. Conclusion

In this study, based on GIS and spatial interpolation techniques, the correlation between lightning activity and topographic features in Inner Mongolia was explored, and a lightning activity prediction model based on the improved DBSCAN algorithm was established. The results show that the improved DBSCAN algorithm performs well in thundercloud center of mass prediction, with an average offset error of only 1.16 km, which is reduced by 39.6% and 62.5% compared with linear extrapolation and least squares methods, respectively. The accuracy of predicting the area of falling mines reaches 89.22%, 83.55% and 83.73% at 8:20-8:25, 8:25-8:30 and 8:30-8:35, respectively, and the false alarm rate is 30.32%, 37.56% and 41.18%, respectively. The topographic characterization found that the frequency of each intensity of lightning and the area share of the interval were basically the same relative to the change in elevation; the northeastern slope was the common susceptibility area of each intensity of lightning, class I and II lightning was also susceptible to occur on the southwestern slope, class III lightning was susceptible to occur on the northwestern slope, and class IV lightning was susceptible to occur on the southern slope; the slope had a significant effect on the density of class I to class III lightning, and they were generally susceptible to occur in the area of the steep slopes, whereas class IV lightning density did does not change with the change of slope. This study can provide a scientific basis for the planning and layout of lightning protection facilities, lightning disaster risk assessment and accurate early warning in Inner Mongolia, which is of great practical significance for improving disaster prevention and mitigation measures and guaranteeing the safe development of the region.

Funding

1. Inner Mongolia Autonomous Region Natural Science Foundation, Research on Cloud-to-Ground Lightning Characteristics Based on Spatiotemporal Clustering (2022MS04003);

2. Basic Research Fund Project for Autonomous Region Universities - Inner Mongolia University of Finance and Economics, Statistical Identification and Data Compilation of Lightning Activity Patterns in Inner Mongolia (NCYWT23049).

References

[1] Cooper, M. A., Holle, R. L., Cooper, M. A., & Holle, R. L. (2019). Current global estimates of lightning fatalities and injuries. Reducing Lightning Injuries Worldwide, 65-73.

[2] Ravaglio, M. A., Küster, K. K., Santos, S. L. F., Toledo, L. F. R. B., Piantini, A., Lazzaretti, A. E., ... & da Silva Pinto, C. L. (2019). Evaluation of lightning-related faults that lead to distribution network outages: An experimental case study. Electric Power Systems Research, 174, 105848.

[3] Li, J., Zhang, X., Li, J., Li, R., Qian, M., & Song, P. (2017). An experimental study of the damage degrees to ancient building timber caused by lightning strikes. Journal of Electrostatics, 90, 23-30.

[4] Janssen, T. A., Jones, M. W., Finney, D., Van der Werf, G. R., van Wees, D., Xu, W., & Veraverbeke, S. (2023). Extratropical forests increasingly at risk due to lightning fires. Nature Geoscience, 16(12), 1136-1144.

[5] Yin, Q., Liu, H., Fan, X., Zhang, Y., Zhuang, Y., Wang, F., ... & Chen, L. (2021). Lightning fatalities in China, 2009-2018. Journal of Agricultural Meteorology, 77(2), 150-159.

[6] Goulden, C. E., Mead, J., Horwitz, R., Goulden, M., Nandintsetseg, B., McCormick, S., ... & Petraitis, P. S. (2016). Interviews of Mongolian herders and high resolution precipitation data reveal an increase in short heavy rains and thunderstorm activity in semi-arid Mongolia. Climatic Change, 136, 281-295.

[7] Doljinsuren, M., & Gomes, C. (2015). Lightning incidents in Mongolia. Geomatics, Natural Hazards and Risk, 6(8), 686-701.

[8] Lu, T., Chen, X., Lei, T., Shen, H., Shi, W., Zhang, L., ... & Miao, L. (2020, July). Research on lightning protection of 500 kV extra-high voltage substation in west inner mongolia power grid. In IET Conference Proceedings CP775 (Vol. 2020, No. 1, pp. 1587-1592). Stevenage, UK: The Institution of Engineering and Technology.

[9] Deng, Y., Li, M., Wang, Y., He, X., Wen, X., Lan, L., ... & Pan, H. (2023). Relationship between lightning activity and terrain in high-altitude mountainous areas. IEEE Transactions on Power Delivery, 38(5), 3561-3570.

[10] Oulkar, S., Siingh, D., Saha, U., & Kamra, A. K. (2019). Distribution of lightning in relation to topography and vegetation cover over the dry and moist regions in the Himalayas. Journal of Earth System Science, 128, 1-17.

[11] Yin, L. Y., Wang, H. Y., Jin, W. J., Zhang, S. D., Wang, W. G., & Mei, H. (2018). Lightning activity characteristics under complex topography in low latitude plateau of China. Applied Ecology & Environmental Research, 16(5).

[12] Santos, A. P. P. D., Ferreira, D. B. D. S., Nascimento Júnior, W. D. R., Souza-Filho, P. W. M. E., Pinto Júnior, O., Lima, F. J. L. D., ... & Tedeschi, R. G. (2024). Lightning under different land use and cover, and the influence of topography in the Carajás Mineral Province, Eastern Amazon. Atmosphere, 15(3), 375.

[13] Wang, X., Zhang, C., Wang, C., Liu, G., & Wang, H. (2021). GIS-based for prediction and prevention of environmental geological disaster susceptibility: From a perspective of sustainable development. Ecotoxicology and Environmental Safety, 226, 112881.

[14] Ahamad, F., Bhutiani, R., & Ruhela, M. (2022). Environmental Quality Monitoring Using Environmental Quality Indices (EQI) Geographic Information System (GIS) and Remote Sensing: A Review. GIScience for the Sustainable Management of Water Resources, 331-348.

[15] Tzavella, K., Fekete, A., & Fiedrich, F. (2018). Opportunities provided by geographic information systems and volunteered geographic information for a timely emergency response during flood events in Cologne, Germany. Natural Hazards, 91, 29-57.

[16] Chen, Z., Chen, R., & Chen, S. (2021). Intelligent management information system of urban planning based on GIS. Journal of Intelligent & Fuzzy Systems, 40(4), 6007-6016.

[17] Huang, F., Yang, J., Zhang, B., Li, Y., Huang, J., & Chen, N. (2020). Regional terrain complexity assessment based on principal component analysis and geographic information system: a case of Jiangxi province, China. ISPRS International Journal of Geo-Information, 9(9), 539.
[18] Antonakos, A., & Lambrakis, N. (2021). Spatial interpolation for the distribution of groundwater level in an area of complex geology using widely available GIS tools. Environmental Processes, 8, 993-1026.
[19] Shahinzadeh, N., Babaeinejad, T., Mohsenifar, K., & Ghanavati, N. (2022). Spatial variability of soil properties determined by the interpolation methods in the agricultural lands. Modeling Earth Systems and Environment, 8(4), 4897-4907.
[20] Liu, L., Lin, Y., Liu, J., Wang, L., Wang, D., Shui, T., ... & Wu, Q. (2017). Analysis of local-scale urban heat island characteristics using an integrated method of mobile measurement and GIS-based spatial interpolation. Building and Environment, 117, 191-207.
[21] Qiao, P., Li, P., Cheng, Y., Wei, W., Yang, S., Lei, M., & Chen, T. (2019). Comparison of common spatial interpolation methods for analyzing pollutant spatial distributions at contaminated sites. Environmental geochemistry and health, 41, 2709-2730.
[22] Xinwu He,Xiqun Liu,Jiajia Liu,Youwen Li,Zhenggang Xu,Ping Mo & Tian Huang. (2025). The T-DBSCAN Algorithm for Stopover Site Identification of Migration Birds Based on Satellite Positioning Data. Biology,14(3),277-277.
[23] Luefeng Chen,Mingdi Ma,Min Wu,Witold Pedrycz & Kaoru Hirota. (2025). Extended multi-kernel relevance vector machine optimized Kriging interpolation for coal seam thickness prediction in coal-bearing strata. Engineering Applications of Artificial Intelligence,145,110093-110093.
[24] Feng Zhang,Yang Yang,Dingyue Lian,Lin Li,Suping Zhao & Chaobo Chen. (2025). An automatic baseline correction method based on reweighted penalised least squares method for non-sensitive areas. Vibrational Spectroscopy,138,103806-103806.